A Multifield Model for Early-Age Massive Concrete Structures: Hydration, Damage, and Creep

Qing Wang, Ph.D.[1]; Xiaodan Ren, Ph.D.[2]; and Roberto Ballarini, Ph.D., P.E., F.ASCE[3]

Abstract: A multifield model of the early-age behavior of massive concrete structures is presented. The hydration process and the thermal evolution are both described through a coupled chemo-thermal model that predicts the degree of hydration and temperature fields that are consistent with experimental measurements. The mechanical model is of the damage–plasticity type and relies on the assumption of additive strains. The classical evolution functions for damage and instantaneous plastic strain are introduced in effective stress space. The extended microprestress-solidification (MPS) theory is implemented to account for the effects of stress, temperature, and degree of hydration on the creep strain. To account for nonlinear creep at relatively high stress, a damage-dependent nonlinear creep function is introduced to couple damage and creep. The autogenous shrinkage and thermal strains are characterized by linear functions of degree of hydration and temperature, respectively. Moreover, the early-age evolutions of strengths and peak strain are also considered to be functions of hydration degree. The model is calibrated and validated through numerical simulations of simple creep tests and a three-dimensional finite element analysis of a massive concrete wall. The results suggest that the proposed model offers promise for the analysis of early-age cracking within massive concrete structures. **DOI: 10.1061/(ASCE)EM.1943-7889.0001851.** *© 2020 American Society of Civil Engineers.*

Author keywords: Massive concrete; Early-age; Temperature; Damage; Creep; Aging effect.

Introduction

The first few days after casting is a critical period for a concrete structure, because early-age concrete exhibits potentially harmful characteristics including (Fig. 1): (1) creep deformation, (2) shrinkage induced by self-desiccation or movement of moisture, (3) thermal expansion caused by the heat of hydration, and (4) an aging produced by the hydration reaction and defined by an increase in stiffness and strength. For massive concrete structures such as nuclear power plants and concrete gravity dams, several features are critical, including early-age shrinkage and thermal deformations that could lead to significant cracking within the newly casted concrete structure. Cracking may aggravate the corrosion of reinforced concrete and, therefore, degrade structural durability and serviceability. Most importantly, cracking and damage increase the probability of leakage for nuclear structures, posing a potential threat to structural security. Generally, early-age behavior presents a major concern for concrete structures, especially for massive ones; therefore, accurate assessment of their performance is needed for structural reliability evaluation.

Numerous studies have been published on the quantitative characterization of the mechanical properties of early-age concrete and several constitutive theories have been proposed. Based on the theory of reactive porous media, Ulm and Coussy (1995, 1996) developed a thermo-chemo-mechanical model to describe shrinkage, thermal changes, and the aging effect. The theory comprehensively reflects the thermo-chemical and chemo-mechanical coupling, but it does not account for creep strain and cracking. In the thermo-chemo-mechanical model proposed by Cervera et al. (1999a, b), which simulates aging, creep, and damage, the degree of hydration and the accompanying heat generation are also calculated according to the reactive porous media theory. The combined damage model and microprestress-solidification (MPS) model is adopted to predict damage and creep strain. However, it mainly focuses on thermal properties but neglects the shrinkage strain. De Schutter (2002a, b) regards degree of hydration as a fundamental parameter to characterize aging, basic creep, thermal expansion, and cracking. A Kelvin chain model is adopted to describe basic creep and the simple smeared cracking relation provided in Model Code 1990 is chosen to account for the cracking phenomenon produced by early-age thermal deformation. However, this model oversimplifies creep and cracking and is unable to sufficiently describe the effect of environmental conditions and the strong nonlinear behavior of the concrete material. Gawin et al. (2006a, b) formulated a hygro-thermo-chemo-mechanical theory to fully account for the hydration reaction and hydro-thermal coupling phenomena. Combining the MPS model and the microplane model together, Luzio and Cusatis (2013) developed the solidification-microprestress-microplane theory that takes into consideration aging, creep, cracking, and particularly hydro-thermo-chemical coupling (Di Luzio and Cusatis 2009a, b). Note that while Gawin's model and the solidification-microprestress-microplane theory both simulate a variety of concurrent deformations at early-age, it is not a viable computational approach for massive concrete structures. Benboudjema and Torr enti (2008) developed a chemo-thermo-mechanical model specifically for massive structures, where the early-age cracking is modeled using a

[1]Student, College of Civil Engineering, Tongji Univ., 1239 Siping Rd., Shanghai 200092, PR China. Email: 1323604728@qq.com

[2]Associate Professor, College of Civil Engineering, Tongji Univ., 1239 Siping Rd., Shanghai 200092, PR China (corresponding author). Email: rxdtj@tongji.edu.cn

[3]Thomas and Laura Hsu Professor and Chair, Dept. of Civil and Environmental Engineering, Univ. of Houston, N127 Engineering Bldg. 1, Houston, TX 77204-4003. ORCID: https://orcid.org/0000-0002-4827-5818. Email: rballarini@uh.edu

Note. This manuscript was submitted on April 15, 2020; approved on May 27, 2020; published online on July 24, 2020. Discussion period open until December 24, 2020; separate discussions must be submitted for individual papers. This paper is part of the ***Journal of Engineering Mechanics***, © ASCE, ISSN 0733-9399.

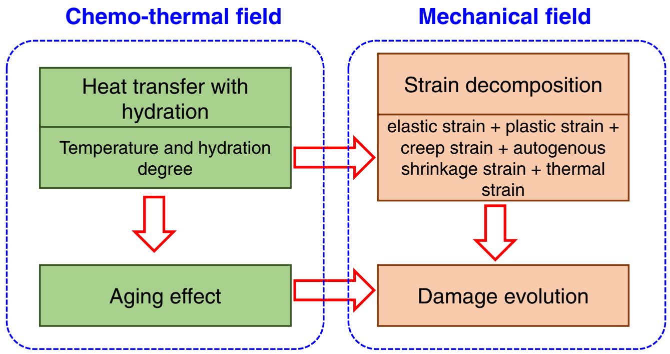

Fig. 1. Early-age concrete characteristics.

simple elastic damage model and the basic creep is simulated with a Kelvin–Voigt chain model. On this foundation, Hilaire et al. (2014) further introduced the microcrack influence parameter into tensile creep modeling and built a new basic creep theory suitable for tensile and compressive loading. In this model, the short-term mechanical behavior is calculated with a scalar-damage model to reflect cracking under tension loading and is not applicable for multiaxial compressive stress states. In summary, significant advances have been made in the understanding of early-age concrete. However, the state of affairs is that the available models are either so comprehensive and complex that their computational cost is prohibitive, or they overlook some of the phenomena involved in early-age concrete.

In this study, a new model for massive concrete structures at early-age is developed, which incorporates the extended MPS model with the classic damage–plasticity model (see Wu et al. 2006; Ren et al. 2015). Focusing on early-age behavior of massive concrete structures, it takes into account damage, instantaneous plastic strain, long-term creep, autogenous shrinkage, thermal deformation, and aging. Due to the influence of the hydration reaction, the temperature of massive concrete structures at early-age could exceed 60°C (140°F). Therefore, the modeling of the chemo-thermal coupling is a critical component of the modeling presented here. Nonlinear creep is taken into account through a nonlinear creep function that reflects the coupling between creep and damage. In addition, the increase of material properties such as strength and peak strain at early-age induced by aging is also considered by modifying the mechanical parameters. It is highlighted that the proposed model comprehensively captures the most important early-age behavior of massive concrete structures including hydration, damage, creep, autogenous shrinkage, and thermal deformation. Concomitantly, the model achieves a trade-off between physical modeling, computational efficiency, and simplicity for use in design environments. The model is systematically validated using experimental data obtained from basic creep tests and from a representative massive concrete wall. The numerical results demonstrate that the proposed model is valid and reliable and offers promise for being used to predict the early-age mechanical behavior of massive concrete structures.

The paper is organized as follows. The next seven sections present the assumptions and equations associated with the numerous physical phenomena. They are followed by the numerical implementation, including the algorithm used to solve the equations and the calibration procedures. Then, on to computational simulation of laboratory experiments on concrete specimens, a case study involving a massive concrete wall, and conclusions.

Chemo-Thermal Model

Chemical Model for Hydration

Hydration of concrete (referring here to the cement hydration involved in ordinary concrete) is an exothermic chemical process accompanied by an increase in stiffness, strength, and other properties. The extent of the hydration process can be described by a nondimensional variable ξ, defined as the degree of hydration. It is defined as the ratio of the current accumulated heat of hydration, L_h, and the total heat of hydration, $L_{\max}$ (which is also referred to as the potential heat of hydration or the latent heat of hydration)

$$\xi = L_h/L_{\max} \tag{1}$$

An estimate of the degree of hydration is necessary to quantify the heat released by the hydration process and the resulting changes in material properties. There are numerous characterizations of the cement hydration reaction (Bentz 1997; Bažant et al. 2003; Lin and Meyer 2009; Rahimi-Aghdam et al. 2017). Considering the trade-off between complexity and precision, the affinity hydration model first proposed by Ulm and Coussy (1995) is adopted here. The evolution of hydration is expressed in the following rate form, where its dependence on temperature is described by the Arrhenius-type law

$$\dot{\xi} = \tilde{\mathrm{A}}(\xi)\exp\left[\frac{Q_\xi}{R}\left(\frac{1}{T_0}-\frac{1}{T}\right)\right] \tag{2}$$

where $\tilde{\mathrm{A}}(\xi)$ denotes the chemical affinity representing the driving force of hydration reaction; Q_ξ denotes the activation energy of hydration process; R is the universal gas constants; and T_0 and T are the reference temperature and the current temperature in Kelvin, respectively. On the basis of Cervera et al. (1999a), Jendele et al. (2014) proposed an approximate expression of the chemical affinity

$$\tilde{\mathrm{A}}_J(\xi) = \mathrm{B}_1\left(\frac{\mathrm{B}_2}{\xi_\infty}+\xi\right)(\xi_\infty-\xi)\exp\left(-\eta\frac{\xi}{\xi_\infty}\right) \tag{3}$$

where B_1, B_2, and η are the material constants controlling the evolution of the hydration reaction; and ξ_∞ is the ultimate hydration degree that depends on the concrete composition. According to Rahimi-Aghdam et al. (2018), the ultimate degree of hydration is a function of the water-to-cement ratio w/c and can be written

$$\xi_\infty = 0.4 + 1.45(w/c - 0.17)^{0.8} \tag{4}$$

Accounting for the influence of the relative humanity on the hydration reaction (Bažant and Najjar 1972), the practical expression of the evolution of degree of hydration is written

$$\dot{\xi} = \tilde{\mathrm{A}}_J(\xi)\beta_h\exp\left[\frac{Q_\xi}{R}\left(\frac{1}{T_0}-\frac{1}{T}\right)\right] \tag{5}$$

$$\beta_h = \frac{1}{1+[a(1-h)]^4} \tag{6}$$

where a is the material parameter and h denotes the pore relative humidity.

Heat Transfer

The behavior of massive concrete structures at early-age is closely related to the temperature. The temperature variation can, on one hand, result in thermal expansion effect; on the other hand, it has a significant impact on the hydration reaction and creep strain.

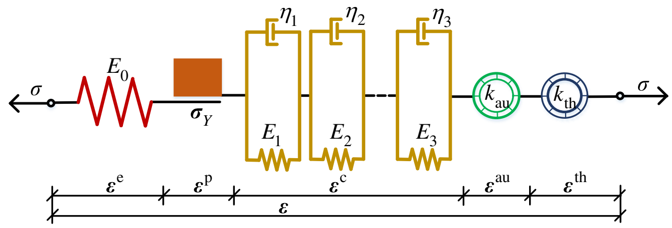

Fig. 2. Schematic representation of the mechanical behavior.

Thus, obtaining the temperature field is essential. Considering heat conduction as the dominant heat transfer process and further introducing additional heat generation due to hydration reaction, the following energy balance equation is adopted

$$\rho C_p \dot{T} = -\nabla \cdot \boldsymbol{q} + L_{\max}\dot{\xi} \tag{7}$$

$$\boldsymbol{q} = -\lambda_t \nabla T \tag{8}$$

where $\boldsymbol{q}$ is the heat flux vector, ρ is concrete mass density, C_p is the special heat capacity, and λ_t is the thermal conductivity. The first term on the right-hand side of Eq. (7) corresponds to the conductive heat flux, which is driven by temperature gradient according to Fourier law. The second term represents the heat generation associated with the hydration reaction.

The heat flux, $\boldsymbol{q}$, on the surface is governed by Newton's law of cooling

$$\boldsymbol{q} \cdot \boldsymbol{n} = B_T(T - T_{\text{ext}}) \tag{9}$$

where B_T is the convective heat transfer coefficient, $\boldsymbol{n}$ is the unit vector in the direction normal to the surface, and T_{ext} is the ambient temperature.

Mechanical Model

Components of Strain

The constitutive law presented in this paper is based on the assumption of small strain additivity

$$\boldsymbol{\varepsilon} = \boldsymbol{\varepsilon}^e + \boldsymbol{\varepsilon}^p + \boldsymbol{\varepsilon}^c + \boldsymbol{\varepsilon}^{\text{au}} + \boldsymbol{\varepsilon}^{\text{th}} \tag{10}$$

where $\boldsymbol{\varepsilon}^e$ is the elastic strain, $\boldsymbol{\varepsilon}^p$ is the instantaneous plastic strain, $\boldsymbol{\varepsilon}^c$ is the creep strain referring to the long-term stress-related deformation, and $\boldsymbol{\varepsilon}^{\text{au}}$ and $\boldsymbol{\varepsilon}^{\text{th}}$ represent, respectively, the autogenous shrinkage strain and thermal strain produced by self-desiccation and temperature variation. As shown in Fig. 2, the basic elements are connected in series. It is noted that the applicability of small strain decomposition has been verified and widely used in concrete constitutive theories (Bažant and Prasannan 1989a; Bažant and Planas 1997; Mazzotti and Savoia 2003; Di Luzio and Cusatis 2013).

Damage–Plasticity Model

The hydration reaction and temperature changes during the early-age of massive concrete structures could create microcracks that result in a decrease in stiffness. This phenomenon is accounted through the damage–plasticity model that has been extensively used and developed (Wu et al. 2006; Ren and Li 2013; Feng et al. 2018b; Feng and Wu 2018). Applying small strain decomposition, the constitutive equation is written

$$\boldsymbol{\sigma} = (\mathbb{I} - \mathbb{D}) : \bar{\boldsymbol{\sigma}} \tag{11}$$

where $\boldsymbol{\sigma}$ is the nominal stress, $\bar{\boldsymbol{\sigma}}$ is the effective stress, $\mathbb{I}$ is the fourth-order identity tensor, and $\mathbb{D}$ is the fourth-order damage tensor that quantifies the reduction in stiffness. In the effective stress subspace, the effective stress in the undamaged state is elastic and is written

$$\bar{\boldsymbol{\sigma}} = \mathbb{E}_0 : \boldsymbol{\varepsilon}^e = \mathbb{E}_0 : (\boldsymbol{\varepsilon} - \boldsymbol{\varepsilon}^p - \boldsymbol{\varepsilon}^c - \boldsymbol{\varepsilon}^{\text{au}} - \boldsymbol{\varepsilon}^{\text{th}}) \tag{12}$$

where $\mathbb{E}_0$ is the fourth-order initial elastic stiffness tensor.

To account for the disparate behaviors in tension and in compression, it is assumed that the stress could be decomposed into tensile (positive) and compressive (negative) components (Wu et al. 2006; Feng et al. 2018a; Ye et al. 2020). Based on the spectral decomposition technique (Simo and Ju 1987a, b), the nominal stress and the effective stress can be written in the following superposition form:

$$\boldsymbol{\sigma} = \boldsymbol{\sigma}^+ + \boldsymbol{\sigma}^-, \qquad \bar{\boldsymbol{\sigma}} = \bar{\boldsymbol{\sigma}}^+ + \bar{\boldsymbol{\sigma}}^- \tag{13}$$

Accounting for the two main failure mechanisms in concrete, the biscalar damage scheme proposed by Wu et al. (2006) is adopted to reflect the differences in degradation between tensile and compressive stress states. The fourth-order damage tensor $\mathbb{D}$ is then simplified as

$$\mathbb{D} = d^+ \mathbb{P}^+ + d^- \mathbb{P}^- \tag{14}$$

where d^+ and d^- are tensile and compressive damage variables, respectively, while $\mathbb{P}^+$ and $\mathbb{P}^-$ are the projection operators corresponding to the tensile and compressive components of the effective stress. The specific damage evolution functions and the empirical damage formulas proposed by Wu et al. (2006) are adopted here.

The iterative nature of classical plasticity theory calculations renders it computationally expensive. Toward the goal of achieving realistic modeling and computational efficiency for massive structures, the phenomenological plastic evolution model proposed by Ren et al. (2015) is adopted. Similar to the decomposition of damage, plastic strain is also split into tensile component $\dot{\varepsilon}^{p+}$ and compressive component $\dot{\varepsilon}^{p-}$

$$\dot{\varepsilon}^p = \dot{\varepsilon}^{p+} + \dot{\varepsilon}^{p-} \tag{15}$$

The tensile and compressive plastic strain components are written

$$\begin{aligned} \dot{\varepsilon}^{p+} &= f_p^+ \dot{\varepsilon}^{e+} = f_p^+ \mathbb{E}_0^{-1} : \dot{\bar{\boldsymbol{\sigma}}}^+ \\ \dot{\varepsilon}^{p-} &= f_p^- \dot{\varepsilon}^{e-} = f_p^- \mathbb{E}_0^{-1} : \dot{\bar{\boldsymbol{\sigma}}}^- \end{aligned} \tag{16}$$

where f_p^+ and f_p^- are the plastic functions corresponding to tensile and compressive plastic strains, respectively. This function could reflect the coupling effect between the plastic strain and damage to some extent and is expressed as

$$f_p^\pm = f_p^\pm(\dot{d}^\pm, d^\pm) = H(\dot{d}^\pm)\kappa_p^\pm (d^\pm)^{n_p^\pm} \tag{17}$$

where the superscript "±" denotes the tensile component "+" and the compressive component "−", and $\kappa_p^\pm$ and $n_p^\pm$ are the empirical parameters controlling the evolution of plastic strain.

Creep Strain and Microprestress-Solidification Theory

The creep strain is introduced using MPS theory, a widely used theory formed by solidification theory and microprestress theory that possesses a solid mechanical foundation (Gasch et al. 2016; Wang and Zhang 2009; Wei et al. 2016, 2019). The solidification theory proposed by Bažant and Prasannan (1989a, b) attributes the

J. Eng. Mech., 2020, 146(10): 04020115

creep aging effect to the gradually occurring hydration reaction. Although the concrete becomes a solid, there exists a significant amount of unreacted cement grains. Over time, the anhydrous cement grains react with the water molecules within the concrete and produce calcium silicate hydrate (C-S-H), which does not age. The additional bonds between the C-S-H particles continuously formed over time and, in turn, they contribute to the aging effect. Consequently, the increase of the hydration product and the polymerization of the C-S-H particles are both responsible for the increase of the macroscopic material properties. The other development within MPS theory is the microprestress theory (Bažant et al. 1997a, b) that can characterize the phenomenon of drying creep and thermal transient creep. Based on the solidification theory, Bažant et al. (1997b) introduced the concept of the microprestress, which on the microscale is a self-equilibrated stress state. This transverse microprestress formed during the initial hydration stage normally acts in the atomic bonds represented by the bridges across the hindered adsorbed water layers. It gradually relaxes with time and is responsible for the long-term aging effect. In addition, the variations of temperature and relative humidity could lead to an imbalance of the microprestress that changes the creep rate (Bažant et al. 2004). Inspired by research in the molecular dynamics community, Rahimi-Aghdam et al. (2018) further developed the extended microprestress-solidification (EMPS) theory that takes into account the inherent physical mechanism of drying creep. As it could preferably reflect the influence of temperature on creep behavior, the EMPS theory is adopted in this work to describe the creep deformation.

In EMPS theory, the stress-related deformation is divided into the instantaneous strain (or elastic strain) and the long-term creep strain. The latter can be further separated into viscoelastic strain and viscous flows. Assuming its age-independence, the elastic strain needs to be modified as follows to match with the instantaneous component in the EMPS theory

$$\boldsymbol{\varepsilon}^e = p_1 \mathbb{E}_{28}^{-}:\bar{\boldsymbol{\sigma}} \tag{18}$$

where $\mathbb{E}_{28}^{-}$ is the fourth-order elastic compliance tensor at 28 days, and p_1 is an empirical parameter that transforms the 28-day elastic modulus $\mathbb{E}_{28}$ into the initial instantaneous elastic stiffness $\mathbb{E}_0 = \mathbb{E}_{28}/p_1$ with age-independent properties.

According to solidification theory, the rate form of viscoelastic strain is expressed as a function of the effective viscoelastic strain rate $\dot{\gamma}(t)$ and the volume growth function $\nu(t)$

$$\dot{\boldsymbol{\varepsilon}}^v = \frac{\dot{\gamma}(t)}{\nu(t)} \tag{19}$$

Using the creep expressions in the B3 and B4 models (Bažant and Murphy 1995; Bažant et al. 2015), the explicit formula of the viscoelastic strain can be further obtained as

$$\boldsymbol{\varepsilon}^v = \bar{\boldsymbol{\sigma}}\{q_2 Q[t_T(t) - t_T(t_0)] + q_3 \ln\{1 + [t_T(t) - t_T(t_0)]^n\}\} \tag{20}$$

where q_2 and q_3 are model parameters related to the cement type, t-t_0 is the loading time, t is the current age, and t_0 is the age at loading. The equivalent time θ is introduced to consider the effect of the hydration process, so that the evolution of $Q(t-t_0)$ is expressed as a function of the equivalent time θ and the loading time t-t_0

$$\theta(\xi) = \left[\frac{0.28}{w/c}\left(\frac{\xi_\infty}{\xi} - 1\right)\right]^{-4/3} \tag{21}$$

$$\frac{dQ(t-t_0)}{dt} = \left(\frac{\lambda_0}{\theta(\xi)}\right)^m \frac{n(t-t_0)^{n-1}}{\lambda_0[1 + (t-t_0)^n]} \tag{22}$$

where λ_0, m, and n are model constants. It is important to note that the effective stress rather than the nominal stress is adopted to calculate the creep strain, since the creep behavior is assumed to occur in the undamaged material. Note that with increasing temperature, the aging process is accelerated and, therefore, the creep rate is reduced. To account for this influence on the viscoelastic strain evolution, the temperature-dependent time function $t_T(t)$ is used in Eq. (20) to replace the actual time t. Consistent with the temperature effect on hydration degree, an Arrhenius type law is also adopted when calculating $t_T(t)$

$$t_T(t) = \int_0^t \beta_T(\tau)d\tau \tag{23}$$

$$\beta_T(t) = \exp\left[\frac{Q_h}{R}\left(\frac{1}{T_0} - \frac{1}{T(t)}\right)\right] \tag{24}$$

where Q_h is the activation energy for the aging process.

The viscous flow strain $\boldsymbol{\varepsilon}^f$ modeled by a dashpot represents the fully unrecoverable creep strain and its evolution is given by

$$\dot{\boldsymbol{\varepsilon}}^f = \frac{\bar{\boldsymbol{\sigma}}}{\eta_M} \tag{25}$$

where η_M denotes the effective viscosity. From the perspective of thermodynamic equilibrium, the effective viscosity could be expressed as the function of microprestress S, temperature T, and relative humidity h

$$\frac{1}{\eta_M} = (aS + b|\dot{\mathrm{S}}|)\beta_\eta(T, h) \tag{26}$$

$$a = a_0\frac{\xi_\infty}{\xi}, \qquad b = b_0\frac{\xi_\infty}{\xi} \tag{27}$$

where model parameters a and b depend on hydration degree and reflect the increase of the effective viscosity with the age, while a_0 and b_0 are material constants; $|\cdot|$ are the absolute value operators. The Maxwell-type rheological model is assumed to govern the relaxation of microprestress with time, and the specific evolution of micropretress could be obtained as

$$\dot{S} + \frac{F_q}{a}\frac{\beta_\eta(T,h)}{\beta_C(T,h)}S^2 = c_1\left(\frac{T}{h}\frac{\partial h}{\partial t} + \frac{T}{h}\frac{\partial h}{\partial T}\frac{\partial T}{\partial t} + \dot{T}\ln(h(t,T))\right) + c_h h^3 \dot{T} \tag{28}$$

The temperature-related variables in the previous equation are calculated as

$$\beta_\eta(T,h) = \exp\left[\frac{Q_\eta}{R}\left(\frac{1}{T_0} - \frac{1}{T(t)}\right)\right]\left(p_0 + \frac{1-p_0}{1 + \left(\frac{1-h}{1-h^*}\right)^{n_h}}\right) \tag{29}$$

$$\beta_C(T,h) = \exp\left[\frac{Q_C}{R}\left(\frac{1}{T_0} - \frac{1}{T(t)}\right)\right] \tag{30}$$

where Q_η and Q_C are both activation energies related to the microprestress process; and p_0, h^*, and n_h are model constants.

Rapidly developed in the initial hydration phase, the initial microprestress is assumed to satisfy the following relationship:

$$S_0 = c_0 q_4 \quad \text{for}\, \xi \leq 0.6\xi_\infty \tag{31}$$

where c_0 and q_4 are material parameters.

Furthermore, considering two distinct creep behaviors under tension and compression, similar to the stress decomposition, we propose that the creep strain could be split into tensile and compressive parts

$$\dot{\boldsymbol{\varepsilon}}^c = \dot{\boldsymbol{\varepsilon}}^{c+} + \dot{\boldsymbol{\varepsilon}}^{c-} \tag{32}$$

where the tensile creep component $\dot{\boldsymbol{\varepsilon}}^{c+}$ and the compressive creep component $\dot{\boldsymbol{\varepsilon}}^{c-}$ are written

$$\begin{aligned}\dot{\boldsymbol{\varepsilon}}^{c+} &= \dot{\boldsymbol{\varepsilon}}^{v+} + \dot{\boldsymbol{\varepsilon}}^{f+}\\ \dot{\boldsymbol{\varepsilon}}^{c-} &= \dot{\boldsymbol{\varepsilon}}^{v-} + \dot{\boldsymbol{\varepsilon}}^{f-}\end{aligned} \tag{33}$$

Owing to limited research on the evolution of the tensile creep strain, the same evolution rules, namely the preceding EMPS theory, are adopted in the subsequent numerical study section to describe the tensile and compressive creep behaviors. Note that the tensile and compressive creep strains are respectively obtained according to the corresponding effective stress components.

The restrained thermal strain, shrinkage, and creep involved in the early-age of massive concrete structures could lead to material nonlinearities. However, EMPS cannot describe nonlinear creep at relatively high stresses because it is based on the assumption that creep strain is linearly proportional to the stress. To account for both linear and nonlinear creep simultaneously, we introduce the damage-dependent influence functions $h^{\pm}(\cdot)$ (Ren et al. 2020) that are defined as a function of the corresponding damage variable

$$h^{\pm}(d^{\pm}) = 1 + c_1^{\pm}(d^{\pm})^{c_2^{\pm}} \tag{34}$$

where $c_1^{\pm}$ and $c_2^{\pm}$ are model parameters that must be fitted using experimental data. In the linear creep phase, concrete experiences negligible damage and, therefore, the damage variable is close to unity. As the stress is increased, damage develops gradually. Through the damage-dependent influence function, the amplification effect caused by the coupling between damage and creep strain could be captured, especially in the nonlinear creep case. Note that there are two terms in the original EMPS theory; the viscoelastic term that represents the behavior of the solid gel, and the viscous flow term that accounts for the irreversible deformation. The creep amplification phenomenon induced by nonlinear creep is due to the development of damage and is not recoverable. Therefore, the nonlinear creep strain could be formulated by amplifying the viscous flow term. This modification of MPS theory, referred to as the damage dependent microprestress-solidification theory (DMPS), leads to

$$\begin{aligned}\dot{\boldsymbol{\varepsilon}}^{c+} &= \dot{\boldsymbol{\varepsilon}}^{v+} + h^{+}(d^{+})\dot{\boldsymbol{\varepsilon}}^{f+}\\ \dot{\boldsymbol{\varepsilon}}^{c-} &= \dot{\boldsymbol{\varepsilon}}^{v-} + h^{-}(d^{-})\dot{\boldsymbol{\varepsilon}}^{f-}\end{aligned} \tag{35}$$

Autogenous Shrinkage Strain and Thermal Strain

During the early-age stage of massive concrete structures, moisture diffusion is much slower than the heat transfer process and the humidity remains nearly constant. Thus, and especially for modern concrete, early-age shrinkage is the result of autogenous shrinkage; dry shrinkage can be ignored in the computational modeling.

As discussed by Mounanga et al. (2006), the early-age autogenous shrinkage due to self-desiccation is directly associated with the hydration process. Although some experimental results (Boulay 2007) show that a slight expansion can be observed during the initial hydration phase, simplified models have been developed in which, above a threshold, a linear relationship between autogenous shrinkage and hydration degree is assumed (Benboudjema and Torrenti 2008; Briffaut et al. 2011; Hilaire et al. 2014). Thus, the evolution of autogenous shrinkage strain could be expressed as

$$\dot{\boldsymbol{\varepsilon}}^{\mathrm{au}} = -k_{\mathrm{au}}\dot{\xi}\mathbf{I} \quad \text{for } \xi > \xi_0 \tag{36}$$

where k_{au} is material constant obtained from experimental data; $\mathbf{I}$ is the second-order identity tensor; and ξ_0 is the hydration degree threshold.

Similarly, a linear relationship between the thermal strain rate and the temperature variation is assumed. Then, the evolution of the thermal strain could be written

$$\dot{\boldsymbol{\varepsilon}}^{\mathrm{th}} = k_{\mathrm{th}}\dot{T}\mathbf{I} \tag{37}$$

where k_{th} is the thermal expansion coefficient that can be assumed constant for a moderate temperature range.

Aging Effect

As the hydration process proceeds, the micropores in concrete are gradually filled with the newly generated C─S─H products (Rahimi-Aghdam et al. 2017; Kai et al. 2019) and, therefore, the microstructure becomes stronger and stiffer; on the other hand, the micropores filling process is accompanied by the increase in the inner microstress. This microstress would lead to the nucleation and growth of microcracks. Consequently, there exists a competition between the volume growth phenomenon and the development of microstress; the former induced by the newly forming hydration products is beneficial for concrete, while the latter is detrimental. According to the research of Ulm et al. (2004), the casted concrete shows highly porous microstructure. Influenced by numerous interparticle pores between anhydrous cement grains, the gradual filling of newly hydrated products plays a dominant role but the increase of the microstress holds a secondary position. Macroscopically, with the hydration process, concrete shows the aging effect, that is a continuous increase of mechanical properties. In the model presented here, the aging is accounted for by establishing proper functional relations with respect to hydration degree.

Stiffness Aging

As previously mentioned, solidification theory could describe the increase of hydration products and the polymerization phenomenon associated with the hydration reaction, which manifests as an increase in macroscale stiffness. In the early version of MPS theory (Bažant et al. 2004), the solidification process governs the evolution of viscoelastic strain that includes the volume growth function $\nu(t)$, representing the aging-related solidified/growth volume fraction of C─S─H up to time t. However, the use of the actual time results in inaccurate descriptions of the hydration reaction process; instead, the equivalent time is adopted, so that the volume growth function in this work is written

$$\frac{1}{v(\xi)} = \left[\frac{\lambda_0}{\theta(\xi)}\right] + \frac{q_3}{q_2} \tag{38}$$

The effective viscoelastic strain rate on the effective area is obtained as $\dot{\gamma}(t) = \nu(\xi)\dot{\boldsymbol{\varepsilon}}^v$ using Eq. (19). Note that the effective viscoelastic strain $\gamma(t)$ is fully recoverable upon unloading but the (nominal) viscoelastic strain $\boldsymbol{\varepsilon}^v$ is partially recoverable as influenced by the volume growth function $\nu(\xi)$.

Strength Aging

Experimental data indicates that concrete tensile and compressive strengths both increase with increasing degree of hydration, especially in the early-age stage. The tensile and compressive strength evolutions are assumed to be connected with the hydration degree by

$$f_t(\xi) = f_{t\infty}\bar{\xi}^{\alpha} \tag{39}$$

$$f_c(\xi) = f_{c\infty}\bar{\xi}^{\beta} \tag{40}$$

where $f_{t\infty}$ and $f_{c\infty}$ are the ultimate tensile and compressive strengths, respectively; and α and β are both material constants that according to experimental data are equal to 0.5 and 0.9, respectively (Table 1), which is consistent with experimental results that the ratio of the compressive and tensile strengths is lower than the ultimate one (Kim et al. 2002; Di Luzio and Cusatis 2013). The nominal hydration degree reads

$$\bar{\xi} = \left\langle \frac{\xi - \xi_0}{\xi_\infty - \xi_0} \right\rangle \tag{41}$$

where $\langle\cdot\rangle = [(\cdot) + |\cdot|]/2$ are the Macaulay brackets; and ξ_0 is the hydration degree threshold corresponding to the critical hydration degree at which concrete becomes solid and achieves significant stiffness and strength. According to Boumiz et al. (1996), it could be assumed to be constant.

Peak Strain Aging

Peak strain is approximately a function of the strength and elastic modulus. Therefore, the peak strain evolution can be assumed to follow the evolutionary equations of stiffness and strength

Table 1. Constant model parameters

Type	Parameter	Value	Unit	Equation
Hydration parameters	Q_ξ	240.5	$\mathrm{J\,mol^{-1}}$	Eq. (5)
	R	8.31441	$\mathrm{J\,mol^{-1}\,K^{-1}}$	Eq. (5)
	T_0	293	K	Eq. (5)
	a	7.5	—	Eq. (6)
Plastic parameters	κ_p^+	0	—	Eq. (17)
	κ_p^-	0.4	—	Eq. (17)
	n_p^+	0.1	—	Eq. (17)
	n_p^-	0.1	—	Eq. (17)
Creep parameters	p_1	0.7	—	Eq. (18)
	n	0.1	—	Eqs. (20) and (22)
	λ_0	1	days	Eq. (22)
	m	0.5	—	Eq. (22)
	Q_h	601.4	$\mathrm{J\,mol^{-1}}$	Eq. (24)
	a_0	$0.005q_4$	—	Eq. (27)
	b_0	$0.00125q_4$	—	Eq. (27)
	F_q	$1.6/q_4$	—	Eq. (28)
	Q_η	481.1	$\mathrm{J\,mol^{-1}}$	Eq. (29)
	Q_C	240.5	$\mathrm{J\,mol^{-1}}$	Eq. (30)
	p_0	0.5	—	Eq. (29)
	h^*	0.75	—	Eq. (29)
	n_h	2.0	—	Eq. (30)
Nonlinear creep parameters	$c_1^\pm$	9.0	—	Eq. (34)
	$c_2^\pm$	0.91	—	Eq. (34)
Aging parameters	ξ_0	0.1	—	Eq. (36)
	α	0.5	—	Eq. (39)
	β	0.9	—	Eq. (40)

$$\varepsilon_t(\xi) = \frac{f_{t\infty}\bar{\xi}^{\alpha}}{E} = \varepsilon_{t\infty}\bar{\xi}^{\alpha} \tag{42}$$

$$\varepsilon_c(\xi) = \frac{f_{c\infty}\bar{\xi}^{\beta}}{E} = \varepsilon_{c\infty}\bar{\xi}^{\beta} \tag{43}$$

where $\varepsilon_{t\infty}$ and $\varepsilon_{c\infty}$ are the tensile and compressive ultimate strains, respectively. Note that the stiffness E is assumed to be independent of the hydration process, since solidification theory is adopted in the creep formulation.

Numerical Implementation

Numerical Algorithm

The proposed model simultaneously takes into consideration (time-independent) elastic-plastic deformation, damage, long-term creep behavior, thermal expansion, autogenous shrinkage, and aging effect. It is truly a comprehensive chemo-thermal-mechanical model. The nonlinearity and complex couplings suggest the use of an explicit computational scheme involving four calculations: (1) degree of hydration; (2) thermal fields and shrinkage; (3) damage–plasticity; and (4) creep.

Given strain increment $\Delta\boldsymbol{\varepsilon}_n$ for a time step $\Delta t_n = t_{n+1} - t_n$, the numerical algorithm updates the stress $\boldsymbol{\sigma}_{n+1}$ at time step t_{n+1}. The first two steps are irrelevant to the level of stress and can be directly evaluated by summation in the difference approximation.

For the damage–plasticity step, a modified operator splitting method (Simo and Hughes 2006) is adopted. The trial effective stress $\bar{\boldsymbol{\sigma}}_{n+1}^{\text{trial}}$ is be obtained as

$$\bar{\boldsymbol{\sigma}}_{n+1}^{\text{trial}} = \mathbb{E}_0 : (\boldsymbol{\varepsilon}_{n+1} - \boldsymbol{\varepsilon}_{n+1}^{\text{au}} - \boldsymbol{\varepsilon}_{n+1}^{\text{th}}) - \mathbb{E}_0 : \boldsymbol{\varepsilon}_n^p - \mathbb{E}_0 : \boldsymbol{\varepsilon}_n^c \tag{44}$$

Based on the spectral decomposition method, the trial effective stress could be decomposed into tension and compression components. According to the tensile and compressive trial effective stress components, the damage variables $d_{n+1}^{\pm}$ are updated using the damage criterion and damage evolution functions. Adopting the damage variables and effective stress, the plastic stress components can further be written

$$\begin{aligned}\Delta\boldsymbol{\sigma}^{p+} &= \mathbb{E}_0 : \Delta\varepsilon_n^{p+} \approx H(d_{n+1}^+ - d_n^+)\xi_p^+(d_{n+1}^+)^{n_p^+}[(\bar{\boldsymbol{\sigma}}^+)_{n+1}^{\text{trial}} - \bar{\boldsymbol{\sigma}}_n^+]\\ \Delta\boldsymbol{\sigma}^{p-} &= \mathbb{E}_0 : \Delta\varepsilon_n^{p+} \approx H(d_{n+1}^- - d_n^-)\xi_p^+(d_{n+1}^-)^{n_p^-}[(\bar{\boldsymbol{\sigma}}^-)_{n+1}^{\text{trial}} - \bar{\boldsymbol{\sigma}}_n^-]\end{aligned} \tag{45}$$

For the creep calculation step, the total creep strain increment consists of viscoelastic and viscous flow strain components that could be integrated in difference form.

At this point, the damage, plasticity, and creep are completely updated, thus allowing the calculation of the effective stress

$$\bar{\boldsymbol{\sigma}}_{n+1} = \mathbb{E}_0 : (\boldsymbol{\varepsilon}_{n+1} - \boldsymbol{\varepsilon}_{n+1}^{au} - \boldsymbol{\varepsilon}_{n+1}^{th}) - \boldsymbol{\sigma}_{n+1}^p - \boldsymbol{\sigma}_{n+1}^c \tag{46}$$

and the updated stress at time step t_{n+1}

$$\boldsymbol{\sigma}_{n+1} = (1 - d_{n+1}^+)\bar{\boldsymbol{\sigma}}_{n+1}^+ + (1 - d_{n+1}^-)\bar{\boldsymbol{\sigma}}_{n+1}^- \tag{47}$$

The complete explicit numerical algorithm is illustrated in Fig. 3.

It is worth noting that the explicit scheme requires no iterations. In addition, Ren et al. (2015) demonstrated that it is very stable under small time increments and that numerical stability could be ensured.

Model Parameter Calibration

The model parameters are of two types; thermal-related and mechanical-related. Thermal-related parameters mainly control the heat transfer process. Mechanical-related parameters can be either constant or must be calibrated using experimental data. All constant parameters, calibration parameters, and thermal-related model parameters are respectively summarized in Tables 1–3.

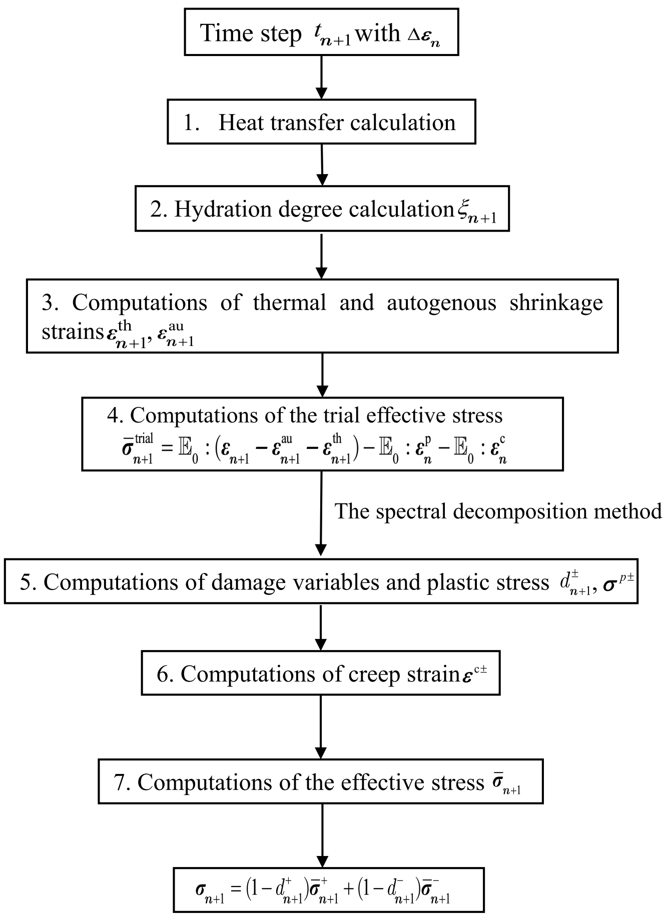

Fig. 3. Explicit algorithm for the chemo-thermo-mechanical model.

Numerical Case Study

Simulation of Basic Creep Test

Aging Creep Tests

The first model verification considers the strength aging and creep aging phenomena using data from an experimental program on the evolutions of the strength, creep, and autogenous shrinkage properties of high-performance concrete (Di Luzio et al. 2015). Cylindrical specimens of 150 mm diameter and 360 mm height and water-to-cement ratio of 0.37 were exposed to a constant temperature 20°C (68°F). Two creep tests were performed at a constant compressive stress equal to 14 MPa; one was loaded at the age of 2 days and the other at 28 days. The related calibration model parameters are listed in Table 2.

Fig. 4 compares the evolution of compressive strength and autogenous shrinkage strain. The simulated compressive strength evolution agrees well with experimental data when plotted in semi-log scale. It is observed that the simulated compressive strength develops rapidly in the first 10 h. Although the experimental autogenous shrinkage evolution exhibits a large scatter, the simulation results have the same trend at early-age. The results suggest that the autogenous shrinkage strain equation is sufficiently accurate for simulating massive structures.

Fig. 5 compares the simulated compliance curves with experiments for basic creep at different loading ages. It is seen that the predictions for 2 and 28 days are both consistent with the experimental measurements.

Creep Tests at Different Temperatures

The experimental tests performed by Umehara et al. (1995) focus on the effect of temperature on the basic creep behavior of early-age concrete. Cylindrical specimens of 100 mm diameter and 200 mm height were subjected to a sustained compression stress of 1.0 MPa at the age of 24 h. Three specimens were cured at 20°C (68°F) for 24 h and then the temperature increased to 20°C, 40°C (104°F), and 80°C (176°F) within the next 6 h. The calibration model parameters are also summarized in Table 2. Fig. 6 compares the simulated

Table 3. Thermal-related model parameters

Parameter	Unit	Equation	Value
C_p	10^6 J kg^{-1} · K^{-1}	Eq. (7)	2.328
λ_t	W m^{-1} K^{-1}	Eq. (7)	3.05
$L_{\max}$	10^6 J m^{-3}	Eq. (7)	154.7
B_T	W m^{-2} K^{-1}	Eq. (9)	3

Table 2. Calibration model parameters

Type	Parameter	Unit	Di Luzio et al. (2015)	Umehara et al. (1995)	Kommendant et al. (1976)	Fahmi et al. (1972)	Wei et al. (2016)	Han et al. (2017)	Massive concrete wall
Hydration parameters	B_1	—	24	24	24	24	24	24	24
	B_2	10^{-5}	1.0	1.0	1.0	1.0	1.0	1.0	1.0
	η	—	5.0	6.9	5.0	6.9	6.5	6.9	5.0
Creep parameters	q_2	10^{-4} MPa^{-1}	0.595	1.606	1.028	1.417	0.995	1.109	1.753
	q_3	10^{-5} MPa^{-1}	0.669	1.846	1.236	3.423	1.245	1.010	0.912
	q_4	10^{-5} MPa^{-1}	1.307	0.926	0.553	3.734	0.568	0.574	1.011
	c_0	10^6 MPa^{-1}	10.0	6.0	6.0	6.0	6.0	5.0	5.0
Autogenous shrinkage	k_{au}	10^{-5}	7.7	7.7	7.7	7.7	7.7	7.7	5.0
Thermal parameters	k_{th}	10^{-5}	1.0	1.0	1.0	1.0	1.0	1.0	1.0

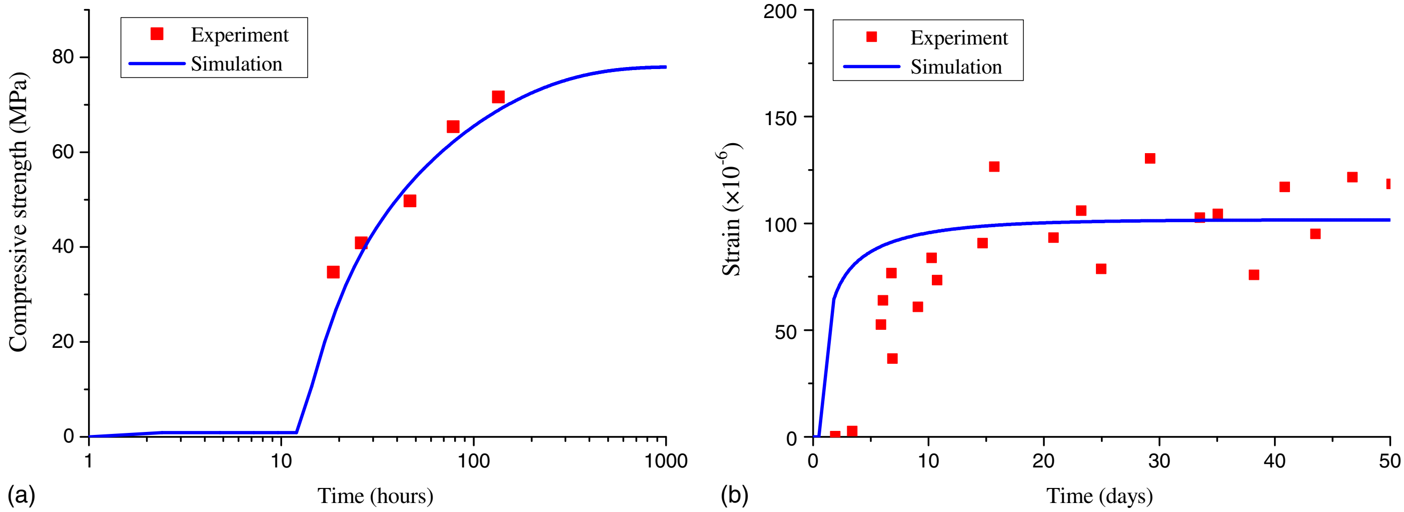

Fig. 4. Evolution of concrete properties: (a) compressive strength; and (b) autogenous shrinkage strain.

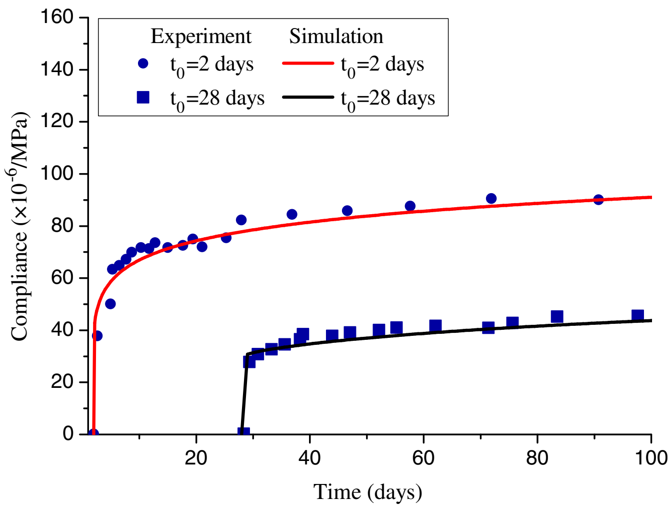

Fig. 5. Comparisons of simulated compliance curves with experimental data at different loading ages.

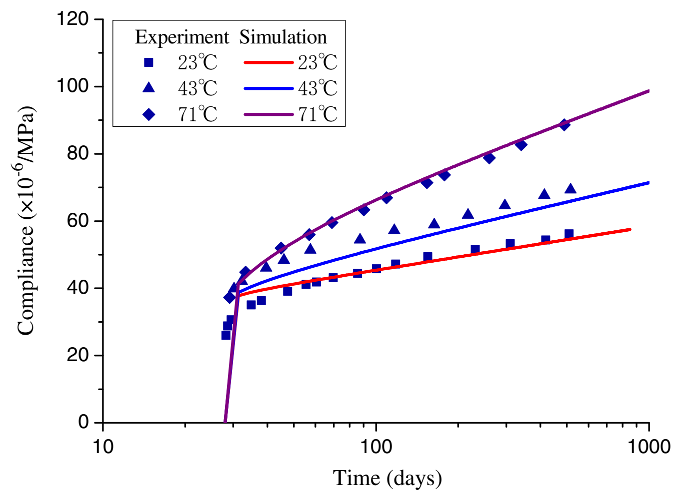

Fig. 7. Comparisons of simulated compliance curves with experimental data under different temperature at the age of 28 days.

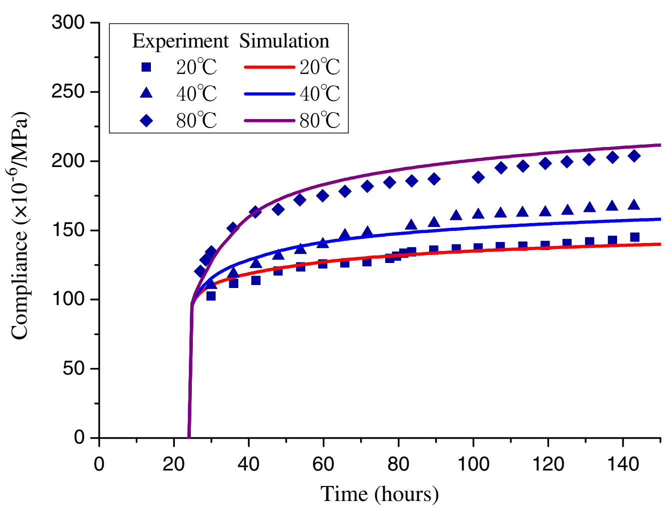

Fig. 6. Comparisons of simulated compliance curves with experimental data under different temperature at the age of 1 day.

compliance curves with the experiment. The numerical results are in very good agreement with experimental data.

The tests carried out by Kommendant et al. (1976) are considered next to simulate the effects of temperature on the creep behavior of mature concrete. The specimens were sealed cylinders of 152.4 mm diameter, 404.6 mm height, water-to-cement ratio of 0.384, and 28-day compressive strength of 46.2 MPa. Three specimens were all cured at 23°C (73.4°F) for 23 days and then heated to 23°C, 43°C (109.4°F), and 71°C (159.8°F), at the rate of 13.33°C (56°F) per day for 5 days. At 28 days, all test specimens were subjected to the sustained axial compressive stress equal to 32% of the 28-day compressive strength. The related calibration model parameters are listed in Table 2. Comparisons of the simulation results with experiment in Fig. 7 show good agreement.

Fahmi et al. (1972) reported experimental data from creep tests on specimens subjected to increasing temperature. The hollow cylindrical specimen was 1,016 mm in height, 152.4 mm in outer diameter, 101.6 mm in inner diameter, mixed with a water-cement ratio of 0.58, and had a 21-day compressive strength of 40.26 MPa.

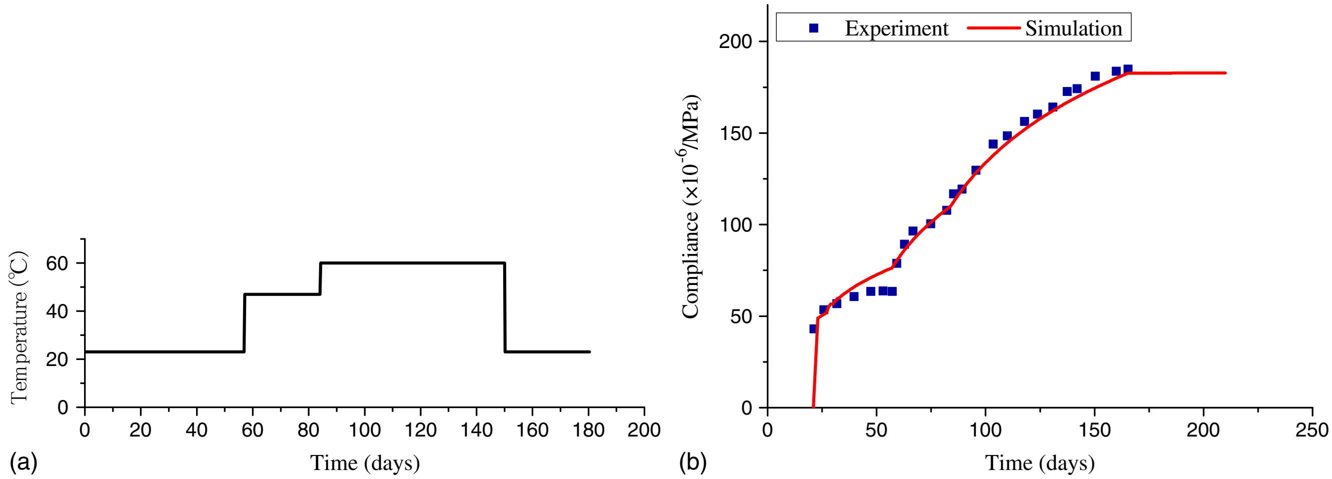

Fig. 8. Comparisons of simulated compliance curves with experimental data under variable temperature loading: (a) temperature loading program; and (b) fit of compliance curve for basic creep.

The temperature was held at 23°C during the curing stage and the subsequent temperature history is shown in Fig. 8(a). At the age of 21 days, the specimen was subjected to an axial compressive stress of 6.3 MPa. The related numerical parameters are listed in Table 2, and comparisons between the simulated basic creep compliance curves and experimental results are shown in Fig. 8(b). It is observed that the model is capable of characterizing basic creep characteristics under variable temperature and capturing the transitional thermal creep phenomenon due to transient temperature variations.

Tensile Creep Tests

The constitutive theory developed here is capable of predicting two different creep behaviors under tensile and compressive loading. In this section, tensile creep experiments performed by Wei et al. (2016) are analyzed to assess the theory's ability to predict basic tensile creep at early-age. Cylindrical specimens of 100 mm diameter and 400 mm height and a water-to-cement ratio of 0.3 were used. The experimentally measured 28-day tensile strength and elastic modulus were 3.9 MPa and 33.0 GPa, respectively. Cured at 23°C, two specimens were exposed to 23°C and 43°C during sustained loading. At the age of 1 day, the specimens were subjected to a tensile stress equal to 70% of the 1-day tensile strength (2.2 MPa). The related numerical model parameters are listed in Table 2.

The predicted tensile creep compliance curves are in good agreement with experimental data, as shown in Fig. 9. Fig. 10 illustrates the importance of the coupling between creep and damage. The linear creep model, which does not account for damage, produces significantly different predictions at both temperatures than the nonlinear model that involves damage. It is important to note that neglecting the coupling significantly underestimates the amount of creep experienced by the concrete.

Creep Tests under Various Stress Levels

The experiments reported by Han et al. (2017) are simulated next to determine the levels of stress for which the present model is applicable. The early-age concrete specimens were 100 × 100 × 300 mm prisms with water-to-cement ratio of 0.39. The 2-day strength and elastic modulus were 16.4 MPa and 12.4 GPa, respectively. Exposed to the temperature of 17°C ± 2°C (59°F–66.2°F), three specimens were loaded with the stress ratios of 0.18, 0.39, and

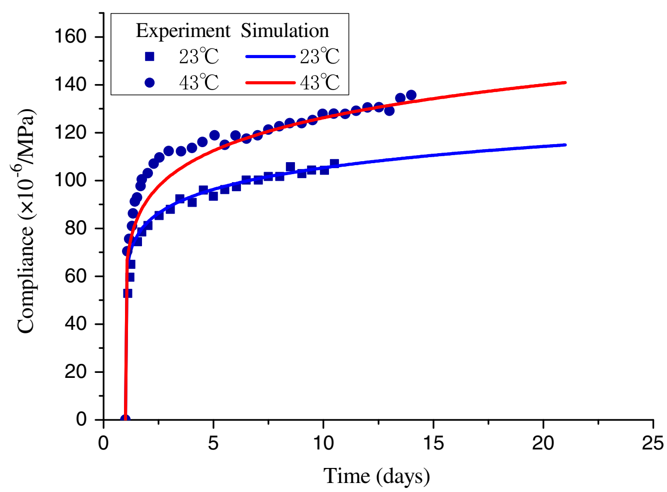

Fig. 9. Comparisons of simulated tension creep compliance and experimental results under different temperatures.

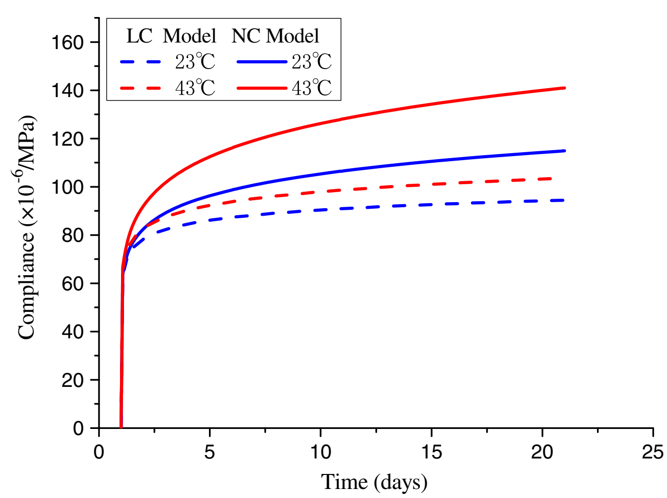

Fig. 10. Comparisons of simulated tension creep compliance using linear creep model (LC Model) and nonlinear creep model (NC Model).

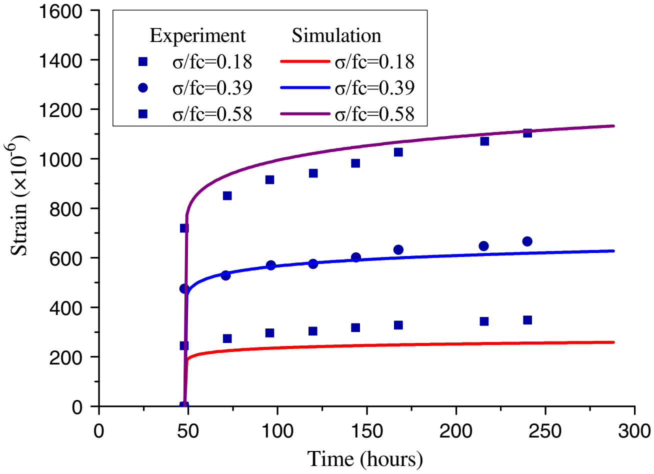

Fig. 11. Comparisons of simulated total strain (removing shrinkage strain) and experimental results under different stress levels.

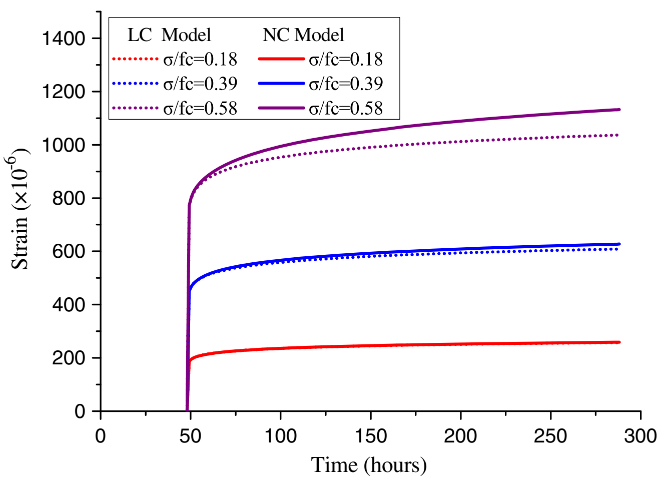

Fig. 12. Comparisons of simulated total strain (removing shrinkage strain) using linear creep model (LC Model) and nonlinear creep model (NC Model).

0.58 at the age of 2 days. The related numerical parameters are reported in Table 2.

Fig. 11 shows that the simulated total strain (excluding the shrinkage strain) are in good agreement with the test data. Fig. 12 shows that for this case, the predictions of the linear creep and the nonlinear creep models are practically the same, especially for low stress levels. These results show that, overall, the damage-dependent influence function introduced in the present model does a good job of predicting linear creep and nonlinear creep.

Early-Age Cracking of a Massive Concrete Wall

This section considers a massive concrete structure in the form of a wall, which was tested to assess the probability of early-age cracking (Ithurralde 1989). The wall was 20 m long, 1.2 m wide, and 1.9 m high and made of normal concrete whose properties are listed in Table 4. Symmetry allows modeling of just one fourth of the actual structure, whose specific geometry is shown in Fig. 13. The thermal parameters that allow the calculation of the temperature field are listed in Table 3. As shown in Fig. 13(c), the following

Table 4. Concrete properties

Properties		Value
Concrete mix	Aggregates (kg m^{-3})	1,871
	Cement (kg m^{-3})	350
	Admixture (L m^{-3})	1.04
	Water (L m^{-3})	195
Mechanical properties	Ultimate stiffness (MPa)	32
	Ultimate tension strength (MPa)	2.5

temperature conditions are assumed: (1) the initial temperature of the wall is maintained at 20°C; (2) the starting temperature of foundation remains at 7°C (44.6°F) and neglecting heat exchange, the temperature of the bottom face of the foundation is fixed at 7°C; (3) ambient temperature varies sinusoidally, with a maximum value of 11°C (51.8°F) at noon and minimum value of 7°C at midnight; (4) ignoring the low heat exchange of the foundation from the surrounding environment, zero heat flux defined by $\boldsymbol{q} \cdot \boldsymbol{n} = 0$ ($\boldsymbol{q}$ is the heat flux and $\boldsymbol{n}$ is the surface normal vector) is assumed on the vertical surface of the foundation; and (5) the concrete foundation is mature and, therefore, its hydration reaction is neglected.

The predictions of the chemo-thermal model are assessed by comparing its predictions of the temperature evolution with the experimental measurements in Fig. 14. The numerical results are in agreement with experimental data, especially during the rising part of the curves; in fact the simulated peak temperature of 58.8°C (137.84°F) is practically the same as the experimentally measured 59°C (138.2°F). Beyond the peak temperature, the simulated temperature is higher than the observed, a difference that could be attributed to the difference between the experimental and simulated ambient temperature. Owing to limited amount of measured temperature data, the sinusoidally varying curve provides a reasonable approximation of the experimental environment. Overall, these results suggest that the present chemo-thermal model is capable of predicting the temperature evolution of massive concrete structures at early-age.

The simulated damage and experimentally observed cracking patterns are displayed in Fig. 15. The experiments (Ithurralde 1989) showed eight major cracks on the whole structure, while three tension-induced localized damage zones were produced in the one-quarter simulation. The simulations indicate significant damage at the edge of the wall that could be attributed to the difference in stiffness between the wall and the foundation. These results show that the model's ability to couple the hydration reaction, creep, thermal deformation, and shrinkage can predict quite well the substantial cracking to which massive concrete structures are susceptible. In addition, the temperature change is a major cause of damage and/or cracking within a massive concrete wall at early-age. In practice, it is necessary to take some measures to decrease the heat generation associated with hydration. Adopting low hydration heat cement and using cooling water piping in high-temperature locations inside the concrete during the construction process are but two examples of damage mitigating strategies.

Conclusions

A chemo-thermo-mechanical model was developed to simulate the behavior of early-age massive concrete structures. The main conclusions can be summarized as follows:

J. Eng. Mech., 2020, 146(10): 04020115

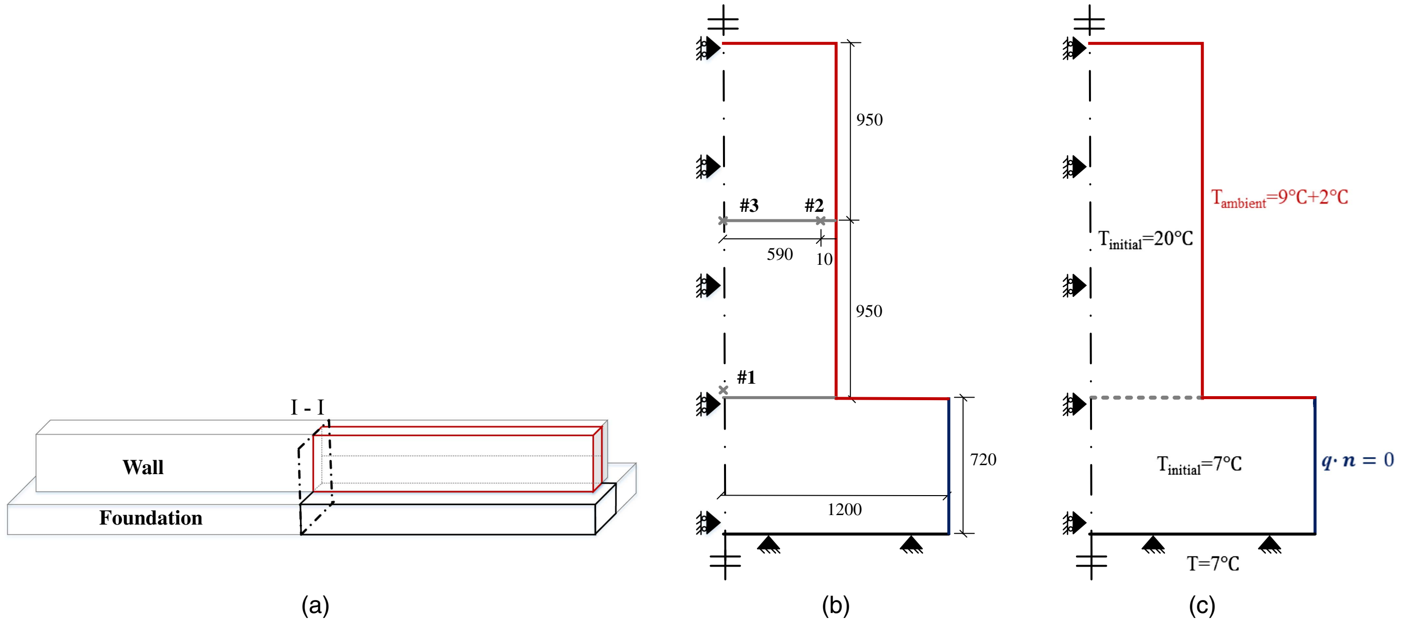

Fig. 13. Geometry of massive concrete wall: (a) schematic representation of the whole test; (b) specific geometry of the cross section I-I; and (c) temperature boundary conditions of the cross section I-I.

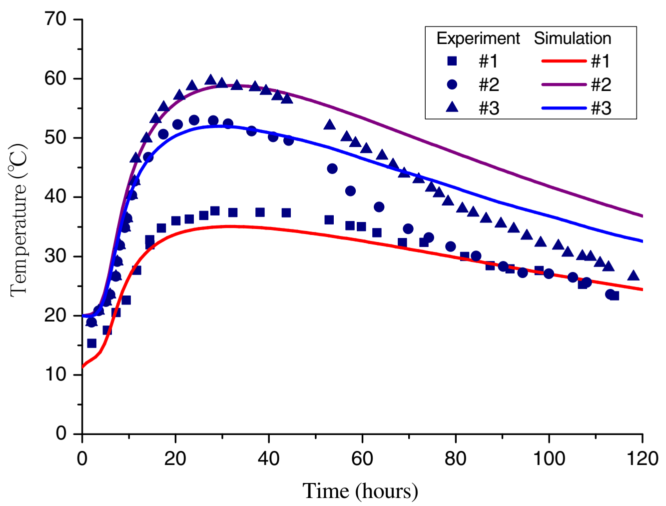

Fig. 14. Comparisons of tested and simulated temperature evolutions at measure points [Fig. 13(b)].

1. Based on the combination of damage–plasticity and a modified version of the DMPS theory, the proposed model is capable of simultaneously characterizing damage, instantaneous plastic strain, long-term creep, autogenous shrinkage, thermal deformation, and aging effects.
2. Variations in the temperature field at early-age were well predicted by implementing the heat transfer process through the coupling of the hydration reaction and thermal conduction.
3. It was demonstrated that the coupling between damage and creep is important to accurately assess the level of creep deformation in massive concrete structures at early-age. Neglecting the coupling leads to an underestimation of creep deformation.
4. The increase in stiffness and strength during the early stage, referred to as aging, is well predicted by using solidification theory and introducing a function of the degree of hydration, respectively.
5. The model predictions are in good agreement with data from a series of uniaxial creep tests, including aging creep tests, creep tests under different temperatures, tensile creep tests, and creep tests under different stress levels.

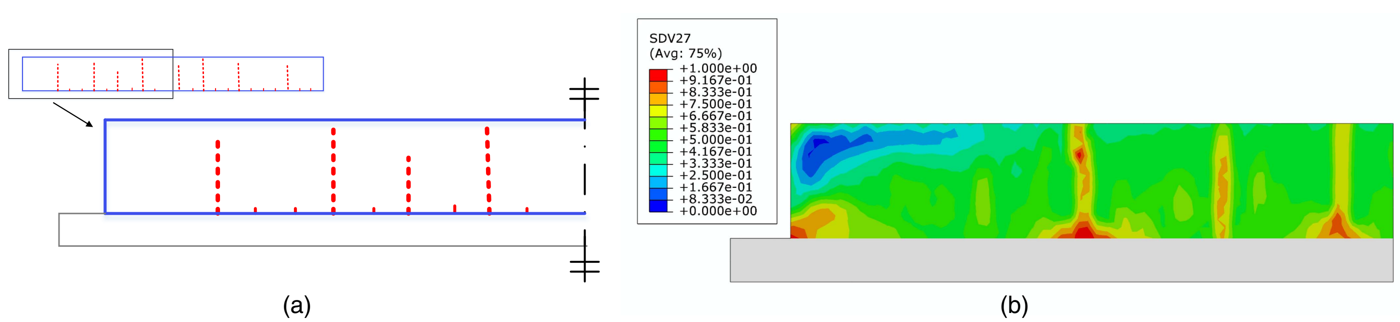

Fig. 15. Comparison of the tested cracking pattern and simulated tensile damage contour: (a) tested cracking pattern; and (b) simulated tensile damage contour.

6. The model achieves its stated desired results. It accounts for complex physical phenomena in a realistic manner but it remains computationally feasible.

Data Availability Statement

All numerical models and computer code generated during the study are available from the corresponding author by request.

Acknowledgments

This work was supported by the National Science Foundation of China (Grant No. 51678439) and Innovation Program of Shanghai Municipal Education Commission (2017).

References

Bažant, Z. P., G. Cusatis, and L. Cedolin. 2004. "Temperature effect on concrete creep modeled by microprestress-solidification theory." *J. Eng. Mech.* 130 (6): 691–699. https://doi.org/10.1061/(ASCE)0733-9399(2004)130:6(691).

Bažant, Z. P., A. B. Hauggaard, and S. Baweja. 1997a. "Microprestress-solidification theory for concrete creep. II: Algorithm and verification." *J. Eng. Mech.* 123 (11): 1195–1201. https://doi.org/10.1061/(ASCE)0733-9399(1997)123:11(1195).

Bažant, Z. P., A. B. Hauggaard, S. Baweja, and F. J. Ulm. 1997b. "Microprestress-solidification theory for concrete creep. I: Aging and drying effects." *J. Eng. Mech.* 123 (11): 1188–1194. https://doi.org/10.1061/(ASCE)0733-9399(1997)123:11(1188).

Bažant, Z. P., M. Jirásek, M. H. Hubler, and I. Carol. 2015. "RILEM draft recommendation: TC-242-MDC multi-decade creep and shrinkage of concrete: Material model and structural analysis. Model B4 for creep, drying shrinkage and autogenous shrinkage of normal and high-strength concretes with multi-decade applicability." *Mater. Struct.* 48 (4): 753–770.

Bažant, Z. P., J. K. Kim, and S. E. Jeon. 2003. "Cohesive fracturing and stresses caused by hydration heat in massive concrete wall." *J. Eng. Mech.* 129 (1): 21–30. https://doi.org/10.1061/(ASCE)0733-9399(2003)129:1(21).

Bažant, Z. P., and W. P. Murphy. 1995. "Creep and shrinkage prediction model for analysis and design of concrete structures-model B3." *Mater. Constr.* 28 (180): 357–365.

Bažant, Z. P., and L. J. Najjar. 1972. "Nonlinear water diffusion in non-saturated concrete." *Mater. Constr.* 5 (1): 3–20. https://doi.org/10.1007/BF02479073.

Bažant, Z. P., and J. Planas. 1997. *Fracture and size effect in concrete and other quasibrittle materials*. New York: CRC Press.

Bažant, Z. P., and S. Prasannan. 1989a. "Solidification theory for concrete creep: I. Formulation." *J. Eng. Mech.* 115 (8): 1691–1703. https://doi.org/10.1061/(ASCE)0733-9399(1989)115:8(1691).

Bažant, Z. P., and S. Prasannan. 1989b. "Solidification theory for concrete creep: II. Verification and application." *J. Eng. Mech.* 115 (8): 1704–1725. https://doi.org/10.1061/(ASCE)0733-9399(1989)115:8(1704).

Benboudjema, F., and J. M. Torrenti. 2008. "Early-age behaviour of concrete nuclear containments." *Nucl. Eng. Des.* 238 (10): 2495–2506. https://doi.org/10.1016/j.nucengdes.2008.04.009.

Bentz, D. P. 1997. "Three-dimensional computer simulation of portland cement hydration and microstructure development." *J. Am. Ceram. Soc.* 80 (1): 3–21. https://doi.org/10.1111/j.1151-2916.1997.tb02785.x.

Boulay, C. 2007. "Développement d'un dispositif de mesure du retrait endogène d'un béton au jeune âge." [In French.] *Actes des 8èmes Journées Scientifiques du RF2B, Montréal* 48–57.

Boumiz, A., C. Vernet, and F. C. Tenoudji. 1996. "Mechanical properties of cement pastes and mortars at early ages: Evolution with time and degree of hydration." *Adv. Cem. Based Mater.* 3 (3–4): 94–106. https://doi.org/10.1016/1065-7355(95)00072-0.

Briffaut, M., F. Benboudjema, J. M. Torrenti, and G. Nahas. 2011. "Numerical analysis of the thermal active restrained shrinkage ring test to study the early age behavior of massive concrete structures." *Eng. Struct.* 33 (4): 1390–1401. https://doi.org/10.1016/j.engstruct.2010.12.044.

Cervera, M., J. Oliver, and T. Prato. 1999a. "Thermo-chemo-mechanical model for concrete. I: Hydration and aging." *J. Eng. Mech.* 125 (9): 1018–1027. https://doi.org/10.1061/(ASCE)0733-9399(1999)125:9(1018).

Cervera, M., J. Oliver, and T. Prato. 1999b. "Thermo-chemo-mechanical model for concrete. II: Damage and creep." *J. Eng. Mech.* 125 (9): 1028–1039. https://doi.org/10.1061/(ASCE)0733-9399(1999)125:9(1028).

De Schutter, G. 2002a. "Finite element simulation of thermal cracking in massive hardening concrete elements using degree of hydration based material laws." *Comput. Struct.* 80 (27–30): 2035–2042. https://doi.org/10.1016/S0045-7949(02)00270-5.

De Schutter, G. 2002b. "Fundamental study of early age concrete behaviour as a basis for durable concrete structures." *Mater. Struct.* 35 (1): 15. https://doi.org/10.1007/BF02482085.

Di Luzio, G., and G. Cusatis. 2009a. "Hygro-thermo-chemical modeling of high performance concrete. I: Theory." *Cem. Concr. Compos.* 31 (5): 301–308. https://doi.org/10.1016/j.cemconcomp.2009.02.015.

Di Luzio, G., and G. Cusatis. 2009b. "Hygro-thermo-chemical modeling of high-performance concrete. II: Numerical implementation, calibration, and validation." *Cem. Concr. Compos.* 31 (5): 309–324. https://doi.org/10.1016/j.cemconcomp.2009.02.016.

Di Luzio, G., and G. Cusatis. 2013. "Solidification–microprestress–microplane (SMM) theory for concrete at early age: Theory, validation and application." *Int. J. Solids Struct.* 50 (6): 957–975. https://doi.org/10.1016/j.ijsolstr.2012.11.022.

Di Luzio, G., R. Felicetti, and L. Cedolin. 2015. "Numerical and experimental study of creep and shrinkage in a high-performance concrete." In Vol. 10 of *Proc., 10th Int. Conf. on Mechanics and Physics of Creep, Shrinkage, and Durability of Concrete and Concrete Structures (Concreep10)*, 128–137. Reston, VA: ASCE.

Fahmi, H. M., M. Polivka, and B. Bresler. 1972. "Effects of sustained and cyclic elevated temperature on creep of concrete." *Cem. Concr. Res.* 2 (5): 591–606. https://doi.org/10.1016/0008-8846(72)90113-5.

Feng, D. C., X. D. Ren, and J. Li. 2018a. "Softened damage-plasticity model for analysis of cracked reinforced concrete structures." *J. Struct. Eng.* 144 (6): 04018044. https://doi.org/10.1061/(ASCE)ST.1943-541X.0002015.

Feng, D. C., and J. Y. Wu. 2018. "Phase-field regularized cohesive zone model (CZM) and size effect of concrete." *Eng. Fract. Mech.* 197 (Jun): 66–79. https://doi.org/10.1016/j.engfracmech.2018.04.038.

Feng, D. C., J. Y. Wu, and Y. Lu. 2018b. "Finite element modelling approach for precast reinforced concrete beam-to-column connections under cyclic loading." *Eng. Struct.* 174 (Nov): 49–66. https://doi.org/10.1016/j.engstruct.2018.07.055.

Gasch, T., R. Malm, and A. Ansell. 2016. "A coupled hygro-thermo-mechanical model for concrete subjected to variable environmental conditions." *Int. J. Solids Struct.* 91 (Aug): 143–156. https://doi.org/10.1016/j.ijsolstr.2016.03.004.

Gawin, D., F. Pesavento, and B. A. Schrefler. 2006a. "Hygro-thermo-chemo-mechanical modelling of concrete at early ages and beyond. Part I: Hydration and hygro-thermal phenomena." *Int. J. Numer. Methods Eng.* 67 (3): 299–331. https://doi.org/10.1002/nme.1615.

Gawin, D., F. Pesavento, and B. A. Schrefler. 2006b. "Hygro-thermo-chemo-mechanical modelling of concrete at early ages and beyond. Part II: Shrinkage and creep of concrete." *Int. J. Numer. Methods Eng.* 67 (3): 332–363. https://doi.org/10.1002/nme.1636.

Han, B., H. B. Xie, L. Zhu, and P. Jiang. 2017. "Nonlinear model for early age creep of concrete under compression strains." *Constr. Build. Mater.* 147 (Aug): 203–211. https://doi.org/10.1016/j.conbuildmat.2017.04.119.

Hilaire, A., F. Benboudjema, A. Darquennes, Y. Berthaud, and G. Nahas. 2014. "Modeling basic creep in concrete at early-age under compressive and tensile loading." *Nucl. Eng. Des.* 269 (Apr): 222–230. https://doi.org/10.1016/j.nucengdes.2013.08.034.

Ithurralde, G. 1989. "The permeability observed by the prescriber." [In French.] In *Colloque Béton à hautes Performances*. , Cachan, France: Ecole Normale Supérieure.

Jendele, L., V. Šmilauer, and J. Červenka. 2014. "Multiscale hydro-thermo-mechanical model for early-age and mature concrete structures." *Adv. Eng. Software* 72 (Jun): 134–146. https://doi.org/10.1016/j.advengsoft.2013.05.002.

Kai, M. F., L. W. Zhang, and K. M. Liew. 2019. "Graphene and graphene oxide in calcium silicate hydrates: Chemical reactions, mechanical behaviors and interfacial sliding." *Carbon* 146 (May): 181–193. https://doi.org/10.1016/j.carbon.2019.01.097.

Kim, J. K., S. H. Han, and Y. C. Song. 2002. "Effect of temperature and aging on the mechanical properties of concrete: Part I. Experimental results." *Cem. Concr. Res.* 32 (7): 1087–1094. https://doi.org/10.1016/S0008-8846(02)00744-5.

Kommendant, G., M. Polivka, and D. Pirtz. 1976. *Study of concrete properties for prestressed concrete reactor vessels, final report—Part II, Creep and strength characteristics of concrete at elevated temperatures*. Rep. No. UCSESM 76-3 Prepared for General Atomic Company. Berkeley, CA: Univ. of California.

Lin, F., and C. Meyer. 2009. "Hydration kinetics modeling of portland cement considering the effects of curing temperature and applied pressure." *Cem. Concr. Res.* 39 (4): 255–265. https://doi.org/10.1016/j.cemconres.2009.01.014.

Mazzotti, C., and M. Savoia. 2003. "Nonlinear creep damage model for concrete under uniaxial compression." *J. Eng. Mech.* 129 (9): 1065–1075. https://doi.org/10.1061/(ASCE)0733-9399(2003)129:9(1065).

Mounanga, P., V. Baroghel-Bouny, A. Loukili, and A. Khelidj. 2006. "Autogenous deformations of cement pastes: Part I. Temperature effects at early age and micro–macro correlations." *Cem. Concr. Res.* 36 (1): 110–122. https://doi.org/10.1016/j.cemconres.2004.10.019.

Rahimi-Aghdam, S., Z. P. Bažant, and G. Cusatis. 2018. "Extended microprestress-solidification theory for long-term creep with diffusion size effect in concrete at variable environment." *J. Eng. Mech.* 145 (2): 04018131. https://doi.org/10.1061/(ASCE)EM.1943-7889.0001559.

Rahimi-Aghdam, S., Z. P. Bažant, and M. A. Qomi. 2017. "Cement hydration from hours to centuries controlled by diffusion through barrier shells of CSH." *J. Mech. Phys. Solids* 99 (Feb): 211–224. https://doi.org/10.1016/j.jmps.2016.10.010.

Ren, X., Q. Wang, R. Ballarini, and X. Gao. 2020. "Coupled creep-damage-plasticity model for concrete under long-term loading." *J. Eng. Mech.* 146 (5): 04020027. https://doi.org/10.1061/(ASCE)EM.1943-7889.0001748.

Ren, X., S. Zeng, and J. Li. 2015. "A rate-dependent stochastic damage–plasticity model for quasi-brittle materials." *Comput. Mech.* 55 (2): 267–285. https://doi.org/10.1007/s00466-014-1100-7.

Ren, X. D., and J. Li. 2013. "A unified dynamic model for concrete considering viscoplasticity and rate-dependent damage." *Int. J. Damage Mech.* 22 (4): 530–555. https://doi.org/10.1177/1056789512455968.

Simo, J. C., and T. J. Hughes. 2006. *Computational inelasticity*. New York: Springer.

Simo, J. C., and J. W. Ju. 1987a. "Strain-and stress-based continuum damage models—I. Formulation." *Int. J. Solids Struct.* 23 (7): 821–840. https://doi.org/10.1016/0020-7683(87)90083-7.

Simo, J. C., and J. W. Ju. 1987b. "Strain-and stress-based continuum damage models—II. Computational aspects." *Int. J. Solids Struct.* 23 (7): 841–869. https://doi.org/10.1016/0020-7683(87)90084-9.

Ulm, F. J., G. Constantinides, and F. H. Heukamp. 2004. "Is concrete a poromechanics materials?—A multiscale investigation of poroelastic properties." *Mater. Struct.* 37 (1): 43–58. https://doi.org/10.1007/BF02481626.

Ulm, F. J., and O. Coussy. 1995. "Modeling of thermochemomechanical couplings of concrete at early ages." *J. Eng. Mech.* 121 (7): 785–794. https://doi.org/10.1061/(ASCE)0733-9399(1995)121:7(785).

Ulm, F. J., and O. Coussy. 1996. "Strength growth as chemo-plastic hardening in early age concrete." *J. Eng. Mech.* 122 (12): 1123–1132. https://doi.org/10.1061/(ASCE)0733-9399(1996)122:12(1123).

Umehara, H., T. Uehara, T. Iisaka, and A. Sugiyama. 1995. "Effect of creep in concrete at early ages on thermal stress." In *Thermal cracking in concrete at early age*, edited by R. Springenschmid, 79–86. London: E & FN Spon.

Wang, Y., and D. Zhang. 2009. "Creep-effect on mechanical behavior of concrete confined by FRP under axial compression." *J. Eng. Mech.* 135 (11): 1315–1322. https://doi.org/10.1061/(ASCE)0733-9399(2009)135:11(1315).

Wei, Y., W. Guo, and S. Liang. 2016. "Microprestress-solidification theory-based tensile creep modeling of early-age concrete: Considering temperature and relative humidity effects." *Constr. Build. Mater.* 127 (Nov): 618–626. https://doi.org/10.1016/j.conbuildmat.2016.10.055.

Wei, Y., J. Huang, and S. Liang. 2019. "Measurement and modeling concrete creep considering relative humidity effect." *Mech. Time-Depend Mater.* 1–17.

Wu, J. Y., J. Li, and R. Faria. 2006. "An energy release rate-based plastic-damage model for concrete." *Int. J. Solids Struct.* 43 (3–4): 583–612. https://doi.org/10.1016/j.ijsolstr.2005.05.038.

Ye, J. Y., L. W. Zhang, and J. N. Reddy. 2020. "Large strained fracture of nearly incompressible hyperelastic materials: Enhanced assumed strain methods and energy decomposition." *J. Mech. Phys. Solids* 139 (Jun): 103939. https://doi.org/10.1016/j.jmps.2020.103939.